Effect of surface treatment of sputtered nickel oxide in inverted perovskite solar cells

Muthu Gomathy M. Pandian,[a,b] Dhruba B. Khadka,[a*] Yasuhiro Shirai,[a*] Masatoshi Yanagida,[a] Saeko Kitamine,[a,c] Amira R. M. Alghamdi,[a,d] Shanthi Subashchandran,[b*] and Kenjiro Miyano,[a]

[a] Photovoltaic Materials Group, Center for GREEN Research on Energy and Environmental Materials, National Institute for Materials Science (NIMS), 1-1 Namiki, Tsukuba, Ibaraki 305-0044, Japan.
[b] Crystal Growth Centre, Anna University, Chennai-600025, Tamil Nadu, India.
[c] Faculty of Science, Kumamoto University, Japan.
[d] Flinders Centre for Nanoscale Science and Technology, Flinders University, PO Box 2100, Adelaide SA 5001, Australia.

Corresponding authors E-mail:
*KHADKA.B.Dhruba@nims.go.jp
*SHIRAI.Yasuhiro@nims.go.jp
*sshanthi@annauniv.edu

Abstract

Nickel oxide (NiO_x) is promising hole transport material for efficient and stable lead halide perovskite solar cell (PSC) due to its promising optoelectronic properties and superior moisture resistivity. Herein, we investigate the effect of surface treatment of sputtered NiO_x film using ethanol (NiO_x-EtOH) in device parameters of PSC. Ethanol treatment of NiO_x facilitates the growth of high-quality perovskite film (larger grain size, better crystallinity, and faster carrier injection). The device with NiO_x-EtOH demonstrated the champion power conversion efficiency of ~13.52% (with open circuit voltage (V_{OC}) ~1.075 V) of 1 cm^2 large-area device. While the device with pristine NiO_x has device efficiency of 11.78% (with V_{OC} ~0.99 V). This report corroborates that the PSC with NiO_x-EtOH improves device performance owing to hydrophilicity, defect passivation of sputtered NiO_x surface, and attenuation of recombination in the perovskite bulk.

Keywords: Sputtering; Nickel oxide; Hole transport layer; Surface treatment; Carrier injection; Morphology; Large area solar cells; Perovskite solar cell.

1. Introduction

Lead halide perovskite solar cells (PSCs) have arisen as low-cost solar energy harvesting materials with high device efficiency from 3.8 to 25.6% in a short period [1]. However, device stability has imposed challenges for commercialization [2]. Since carrier transport layers affect perovskite bulk properties, interface quality, and device stability [3–6], the engineering of carrier transport layers has gained significant attention for resolving the issue of PSCs [7].

Owing to high hole mobility, excellent optophysical properties, and air stability, nickel oxide (NiO_x) has gained significant attention as a hole transporting layer (HTL) [8]. PSCs with NiO_x HTLs have demonstrated a competitive power conversion efficiency (PCE) [9] and stability under a variety of stressors, including humidity damp heat test, and operational stability at elevated temperatures [10,11]. Many reports have used a variety of processing routes for NiO_x deposition; (i) wet deposition technique such as nanoparticles coating [5,12], spray pyrolysis [13], and sol-gel [14] and (ii) dry deposition technique such as atomic layer deposition [10], and sputtering.[15,16] Among these techniques, sputtering deposition is more suitable for large area deposition with precise control of NiO_x composition [17,18], It reported that the NiO_x consists of multiple composites such as Ni_2O_3, and Ni-OH derivatives induced by oxidation of NiO_x which leads to p-type conductivity [19,20]. The surface chemistry and crystallinity are crucial for tuning the electrical properties of NiO_x film [16,21]. The surface treatments and doping on NiO_x film have been widely used for tuning the film properties that have demonstrated a significant effect on the performance of the PSCs [9,12,22–24]. Therefore, it is important to investigate the surface treatment effect on NiO_x film for optimizing carrier transport properties and interfacial contact to get high efficiency and stable PSC.

In this report, we present the cost-effective and facile surface treatment of NiO_x film sputtered without annealing. We selected absolute ethanol for the solvent treatment of sputtered NiO_x surfaces for the fabrication of large-area PSC devices. The film properties of as-sputtered and ethanol-treated NiO_x film were analyzed by evaluating film morphology, optophysical properties, and surface chemistry. We fabricated inverted PSCs using NiO_x (with and without ethanol-treated) as HTL. The device with ethanol-treated NiO_x (NiO_x-EtOH) showed improved device performance with higher reproducibility. We found that the NiO_x-EtOH film affects not only the morphology of NiO_x and interface or bulk quality of perovskite film but also the carrier dynamics of devices as a consequence of interfacial modification. This work has underscored the effects of ethanol treatment on sputtered NiO_x film and its impacts on PSC focusing on the surface chemistry and photophysics.

2. Materials and methods

2.1. Materials

Unless otherwise mentioned, all chemicals were obtained from commercial vendors and used as received. Methylammonium halides (MAI, MACl; >99%, sigma aldrich) and PbI_2 (>98%, wako chemical company), 5-aminovaleric acid hydroiodide (5-AVAI; (>99%, TCI) were used for perovskite precursor solution. [6,6]-Phenyl C_{61} butyric acid methyl ester (PCBM) (Sigma-Aldrich, 99% purity) was used for electron transport layer (ETL) deposition. Aluminum doped zinc oxide (AZO) nanoparticle ink (Nanograde, N-21X, Avantama) was used to prepare the AZO layer.

2.2 Device fabrication

We prepared NiO_x film by sputtering deposition technique following our previous reports [25]. In brief, the pre-cleaned ITO substrates were loaded in the deposition chamber and evacuated until $<2\times10^{-3}$ Pa then pure argon gas was introduced at the rate of 20 standard cm^3/min. The deposition was carried out in an argon gas pressure of 3.5 Pa and rf power supply of 50 W for 20 min at room temperature. We used NiO_x target (99.9% pure) from Kojundo Chemical Laboratory Co. Ltd, Japan. The sputtered NiO_x film was dipped into ethanol for surface treatment for 5 - 20 min (EtOH treatment) (Fig. 1). Then NiO_x film was dried by blowing nitrogen gas.

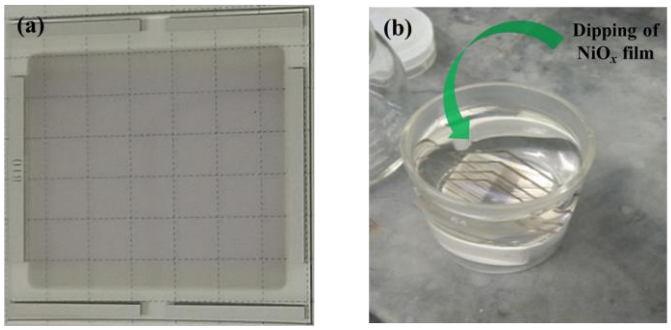

Fig. 1. Photos of sputtered NiO_x deposited on ITO (a). Sputtered NiO_x thin films dipped in ethanol (process of ethanol treatment on the surface of NiO_x film) (b).

For the fabrication of perovskite films, the PbI_2 solution was prepared by dissolving PbI_2 (500 mg/ml) + 5-AVAI (3 mg/ml) in a mixture of anhydrous DMF/DMSO (5:1 ratio) at 500 rpm/ 70^{o}C for 12 hours. The MAX (MAI and MACl) solution (50 mg/ml; 19:1 ratio) in ethanol at 300 rpm/ 50^{o}C for 12 hours. The PbI_2 precursor solution was spin-coated at 3000 rpm for 90

s and the MAX precursor solution (a mixture of MAI + MACl) was subsequently spun onto the PbI_2 layer at 4000 rpm, for 30 s. Those as-grown $CH_3NH_3PbI_{3-x}Cl_x$ (x= 0.002) perovskite films were simply placed on the hot plate with MACl powder covered with a petri dish at 100 ^oC (30 min) for crystallization [26]. Then, PCBM (2 wt% in chlorobenzene) was spin-coated on perovskite film (700 rpm for 30 s and 4000 rpm for 10 s) and annealed at 100 ^oC for 15 min. A thin AZO layer (~25 nm) was deposited at 2500 rpm for 25 s and annealed at 100 ^oC for 10 min. Finally, 140 nm of Ag was thermally evaporated at a pressure $<10^{-4}$ Pa to complete the device structure. Devices were sealed by encapsulation glass and UV-curable resins (UV-RESIN XNR5516Z; Nagase ChemteX, Japan) before the subsequent measurement in ambient conditions. We fabricated the inverted structure planar devices; ITO/NiO_x/perovskite/PCBM/AZO/Ag and encapsulated them as described in our previous reports [27]. The details of the precursor solution and device fabrication can be found in the earlier reports [26,27].

2.3 Materials and Device Characterizations

We used a Rigaku X-ray diffractometer (CuKα radiation, λ= 1.54 Å) to measure X-ray diffraction (XRD) patterns Bragg-Brentano θ-2θ configuration at room temperature. The morphology of films and cross-sectional images were taken by a high-resolution scanning electron microscope (SEM) at 5 kV accelerating voltage (Hitachi, S-4800, SU8000). The absorption spectra and work function were measured by UV-vis spectrometer (Shimadzu, 2600) and photoelectron spectrometer (Riken Keiki, AC-3). X-ray photoelectron spectroscopy (XPS) spectra were obtained using a Versa Probe II (ULVAC-PHI, Japan). XPS with a nonmonochromatic source was measured (Al Kα; 1486.6 eV, spot size 10-300 μm) at a pass energy of 187.85 eV (1.5 eV step size) for the survey scan and pass energy 46.95 eV (0.1 eV step size) for the fine scan with spot size 100 μm. The XPS spectra were calibrated with the binding energy of 284.8 eV for C1s. The baseline correction was carried out to make a linear background (linear method) using origin software. The XPS spectral fitting was done with the Voigt function fixing the characteristics XPS peaks for respective chemical species and their full width at half maxima using origin software. The surface hydrophobicity of film was measured using contact angle measurements (AST, VCA Optima XE, nano-bio platform). Briefly, a 1.6 μL drop of deionized water was placed on the film. The carrier lifetimes were measured with a fluorescence lifetime spectrometer (Quantaurus-τ from Hamamatsu-Photonics K. K.) equipped with ~405 nm laser diode (typical peak power of 400 mW) at 200 kHz repetition rate. The current density–voltage (J–V) curves were measured at the scan rate of 0.05

V/s under 1 sun with an AM1.5G spectral filter (100 mW/cm^2) coupled with a maximum power point tracking system (Systemhouse Sunrise Corp.). The light intensity is calibrated by a silicon diode (BS-520BK).

3. Results and discussion

We studied the film properties of ethanol treatment of NiO_x film deposited by sputtering without annealing. The thickness of NiO_x film is ~20 nm. Figs. 2a-c show SEM images of ITO, sputtered-NiO_x, and NiO_x-EtOH thin films. One can see the closely packed, uniform surface of the as-sputtered NiO_x thin film with an average crystallite size of ~11 nm. The NiO_x-EtOH shows a modification in surface morphology with a large crystallite size. XRD patterns (Fig. 2d) of the NiO_x films deposited on ITO substrate (# -XRD peak) show the cubic structure characteristic dominant peaks located at 35.31°, 38.09°, and 44.3° corresponding to the crystal orientations of (111), (101), and (200), respectively. These results are well-matched with reports [28,29]. Moreover, we noticed only (111) peaks remained dominant in NiO_x-EtOH film indicating orientational modification coupled with surface morphology. It has been reported that the conductivity of NiO_x film with (111) orientation is higher than that of (200) or mixed orientations [21] indicating a benefit of ethanol treatment of NiO_x. Fig. 2e shows transmittance spectra of glass, ITO, and NiO*x* film deposited on ITO. We noticed transmittance of ~80% in the range of 400-800 nm wavelength for the pristine film. The NiO_x-EtOH film shows a slightly higher transmittance indicating improved optophysical properties. It could be correlated to the large grain size in NiO_x-EtOH (Fig. 2c) which might decrease the light scattering with modified grain boundaries in film.

We also measured the contact angle to evaluate the surface wettability of films. Figs. 2f-h show the contact angle measurement of ITO, as-sputtered NiO_x, and NiO_x-EtOH films. The contact angle of water on ITO (~17.5^o) indicates a super hydrophilic surface. The water contact angle of as-sputtered NiO_x is ~59.6^o while that for NiO_x-EtOH decreases to ~45.8^o. It suggests that ethanol treatment of sputtered NiO_x results in a more hydrophilic surface which plays a vital role in fabricating high-quality perovskite film.

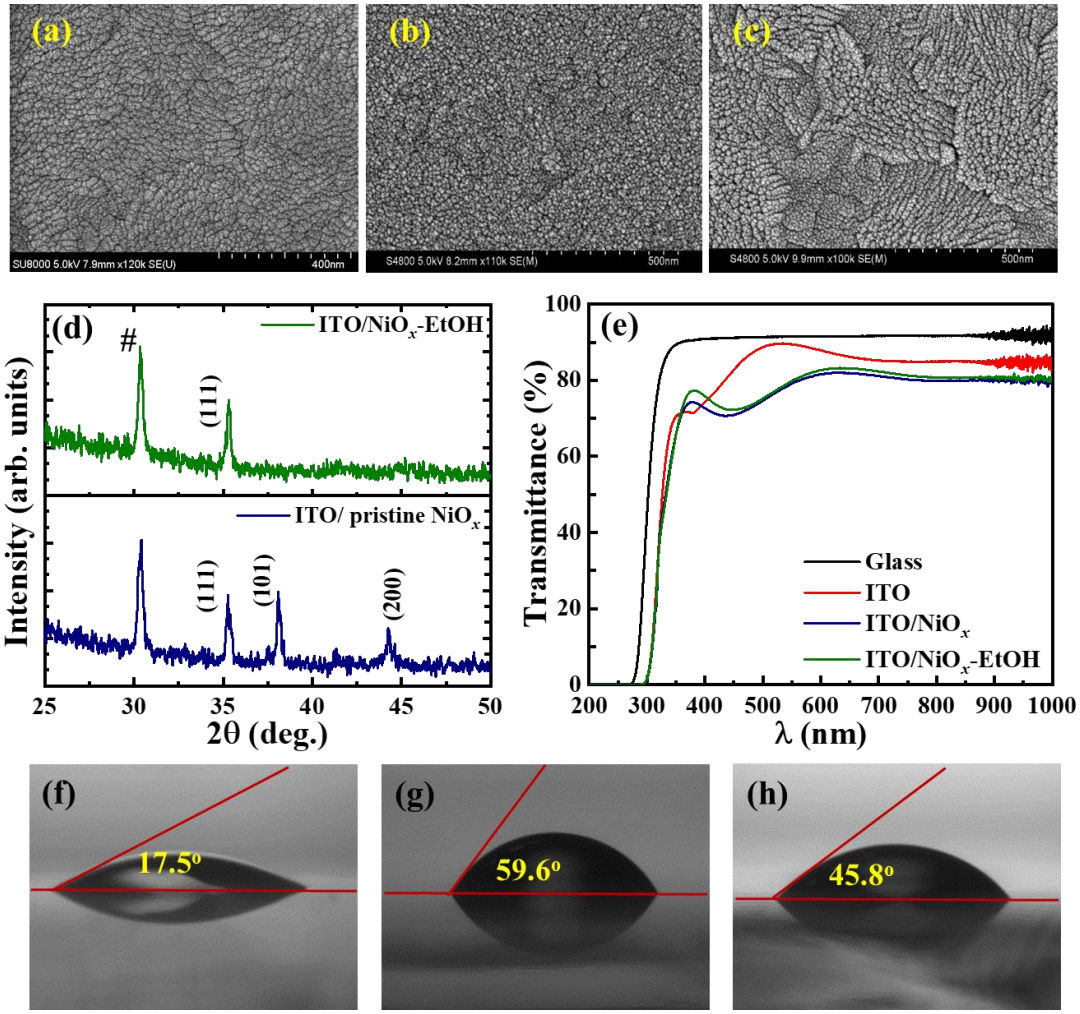

Fig. 2. SEM surface morphology of (a) ITO substrate, sputtered NiO_x (b) without and (c) with ethanol treatment. XRD patterns (# denotes ITO) (d) and transmittance spectra (e) of respective films. Water contact angles on different surfaces; (f) ITO, (g) ITO/NiO_x, (h) ITO/NiO_x-EtOH.

Furthermore, the photoelectron spectra of respective films (Figs. 3a, b) show an increase in the HOMO level of the post-ethanol treated NiO_x film (5.40 eV $\pm$ 0.02 eV for pristine NiO_x to 5.49 $\pm$ 0.02 eV for NiO_x-EtOH). It could induce a small spike at NiO_x-EtOH and perovskite interface in device structure that is benign for effective carrier dynamics in thin film solar cells [30].

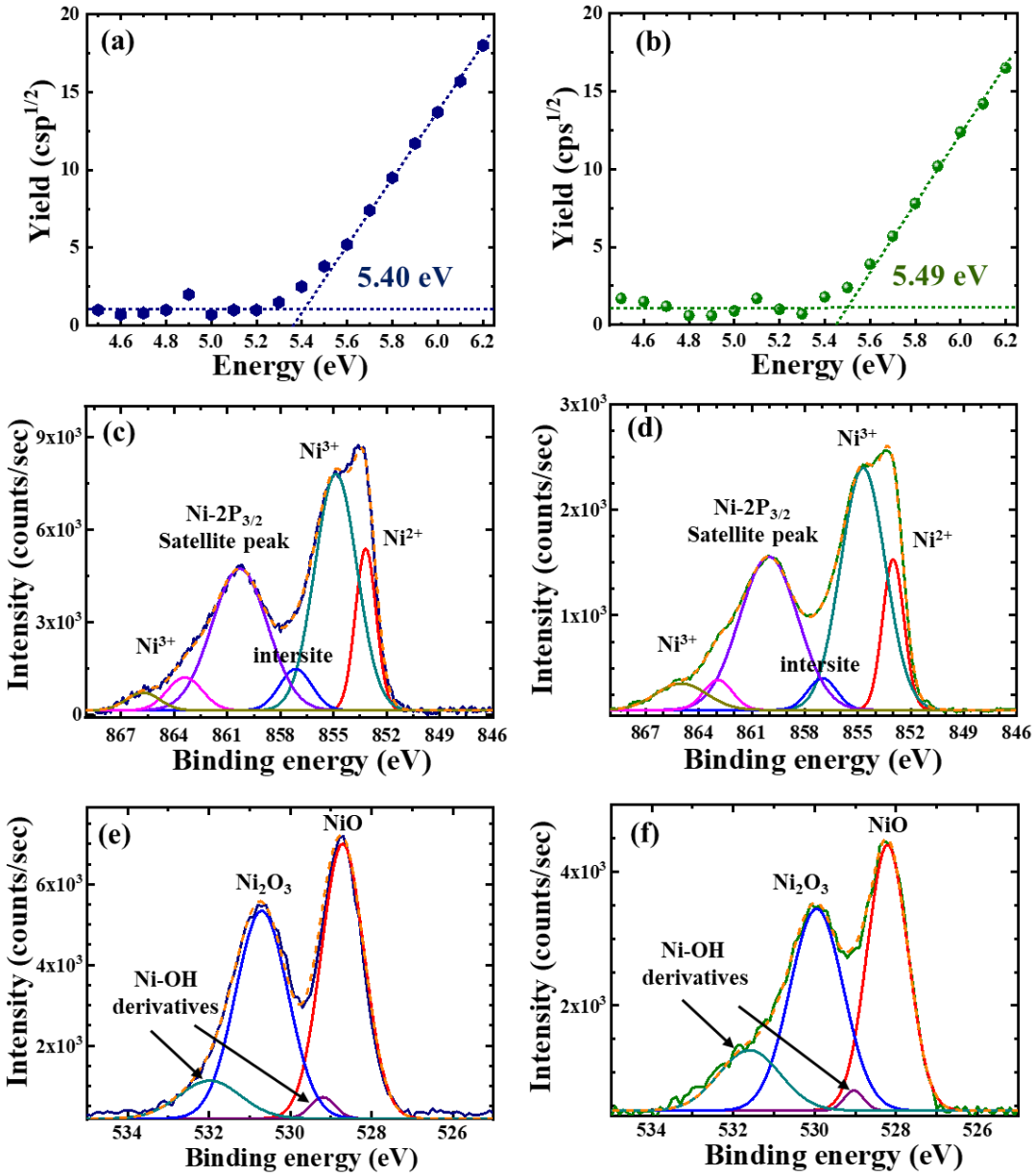

Fig. 3. Photoelectron spectra of NiO_x [(a) as-sputtered and (b) with ethanol treatment]. Ni 2p XPS spectra of (c) as-sputtered, (d) ethanol- treated NiO_x films, and O1s XPS spectra of respective films (e) and (f).

To investigate the effect of ethanol treatment on surface chemistry, X-ray photoelectron spectroscopy was performed and the characteristics spectra were analysed as depicted in Fig. 3. The XPS spectra of the Ni 2p core (Figs. 3c, d) assign the characteristics peaks. The characteristic peaks of the XPS spectra were fitted with the Voigt function. A broad peak centred at ~860.7 eV corresponds to the shakeup process in the NiO_x structure that is referred to as the satellite peak. The peaks centred at ~853.4, ~855.3, and ~857.2 eV correspond to Ni^{2+}, Ni^{3+}, and Ni-intersite, respectively [20,31,32]. The ionic composition of NiO_x film was

evaluated by calculating the integral area of the fitting curve of the XPS spectra. The Ni^{3+}/Ni^{2+} ratio of NiO_x films shows a higher value for NiO_x-EtOH film (~3.37) compared to as- sputtered NiO_x (~2.97). It has been documented that a higher amount of Ni^{3+} ionic species improve the surface wettability of NiO_x film [20]. Our result XPS result is consistent with water contact angle results (Figs. 2g-h). Similarly, O 1s -core spectra (Fig. 3e, f) were fitted to four peaks centred at ~529.4, ~530.8, ~529.4, and ~531.9 eV corresponding to NiO, Ni_2O_3, and Ni-OH derivatives ($Ni(OH)_2$, NiOOH), respectively. These results are in good agreement with previous reports [9,20]. It is found that the ethanol treatment increases the concentration of Ni-OH derivatives species resulting dipolar surface. Importantly, accounting for the higher percentage of Ni_2O_3, and Ni-OH derivatives, it has been reported to contribute to increasing work function and enhancing the carrier transport dynamics [32,33]. This is supported by the photoelectron spectra (Figs. 3a, b) and time-resolved photoluminescence (TRPL) results (discussed below).

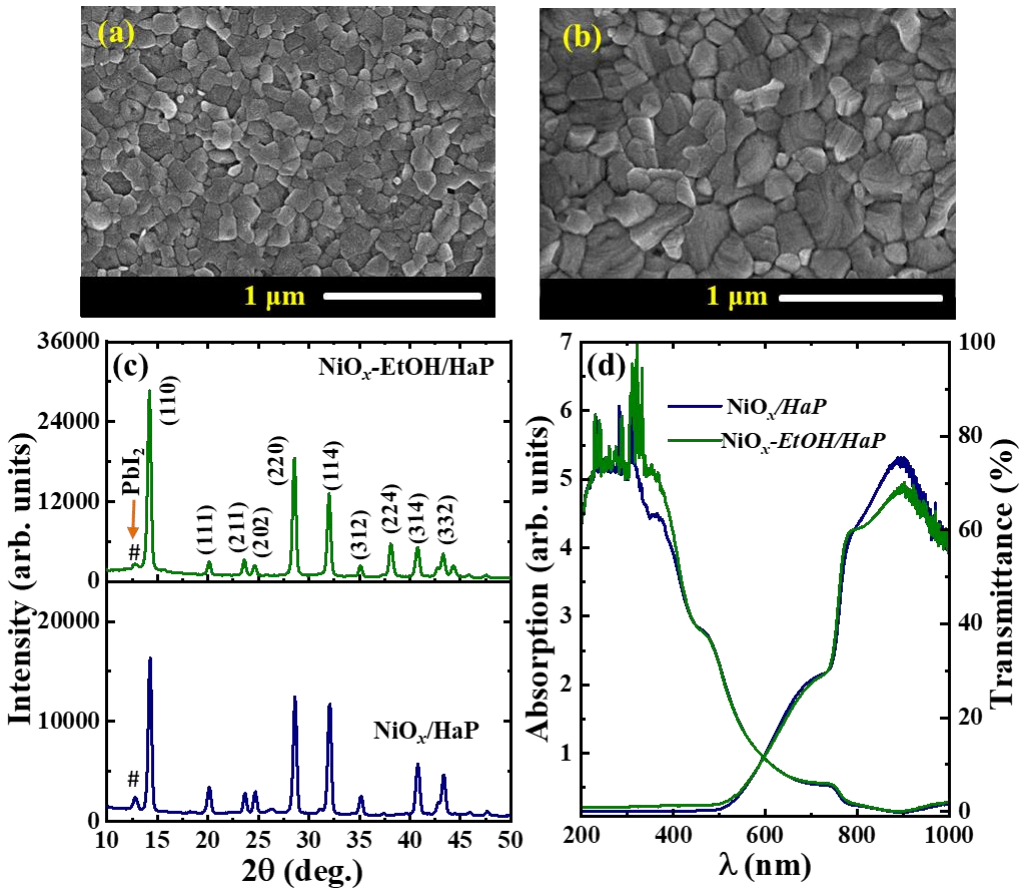

Fig. 4. SEM surface morphology perovskite film deposited on sputtered NiO_x without (b) and with ethanol treatment (b). XRD patterns (c) and UV-vis absorption/transmittance (d) of respective films.

To examine the effect of ethanol treatment of sputtered NiO_x on perovskite film, we investigated the growth properties of the films. The SEM images of the perovskite films grown on pristine or NiO_x-EtOH film are shown in Figs. 4a, b. One can see a well-grown pinhole-free surface morphology of the perovskite film. The perovskite film on NiO_x-EtOH grows with a larger grain size ranging from 150-600 nm with an average size of ~300 nm. While the perovskite grains on pristine NiO_x have comparatively smaller grain sizes ranging from 50-300 nm. It has been reported that large grain size reduces grain boundary defects which is beneficial for enhancing device performance [26,34]. Fig. 4c shows the XRD patterns of perovskite films with characteristic orientations [4,27]. The XRD patterns of the perovskite film grown on the NiO_x-EtOH film exhibited a relatively higher intensity of (110) and (220) crystal orientations suggesting better crystallinity of perovskite film. We found relatively diminished PbI_2 peak intensity for the perovskite film grown on NiO_x-EtOH film which is beneficial for device performance and stability [35].

Furthermore, the optophysical properties were measured by UV-vis spectroscopy. No difference was noticed in the absorption and transmittance spectra of perovskite films deposited on respective NiO_x substrates (Fig. 4d) at the band edge. The optical band edge of perovskite bulk is estimated to be ~1.58 $\pm$ 0.02 eV for both films. One can notice higher absorption in the lower wavelength regime that is correlated to improvement in interface quality with NiO_x-EtOH and perovskite.

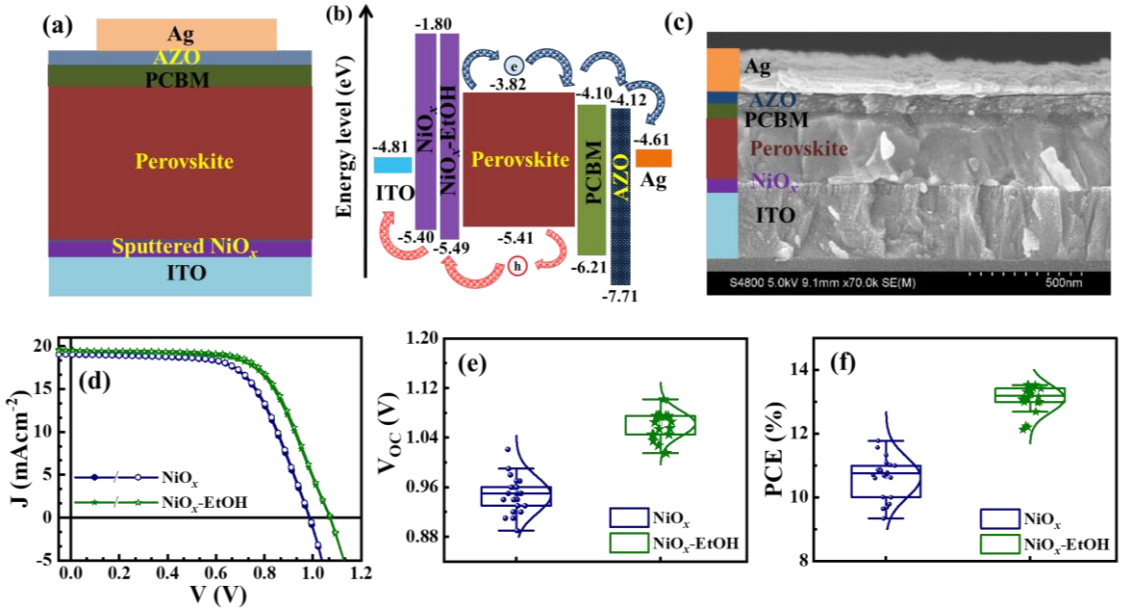

Fig. 5. Schematic diagram of device architecture (a). Energy band diagram of the device (b). Cross-sectional image of PSC (c). Current density-voltage (*J-V*) curves of PSCs with pristine

NiO_x and NiO_x-EtOH as HTL (■forward /□ reverse scan direction; inset 1 cm^2 device area) (d). Statistics of device parameters; V_{OC} (e), and *PCE* (f).

Table 1. Photovoltaic performance of the fabricated device using sputtered NiO_x; without and with the surface by ethanol. Here, V_{OC} -open circuit voltage, J_{SC} -short circuit current density, *FF*- fill factor.

NiO_x-condition	J_{sc} (mA/cm^2)	V_{oc} (V)	*FF*	*PCE* (%)	Diode ideality factor (*n*)	PL lifetime	
						t_1 (ns)	t_2 (ns)
Pristine	18.94	0.99	0.628	11.78 ± 0.64	2.18	4.68	43.31
NiO_x-EtOH	19.48	1.075	0.646	13.52 ± 0.35	1.61	2.56	54.28

To evaluate the photovoltaic performance, we fabricated PSCs using NiO_x HTL. Fig. 5a shows the schematic diagram of the inverted structure of PSC with an energy band diagram (Fig. 5b) having PCBM as an ETL coupled with a thin AZO as an electron selective layer beneath the Ag electrode. In the energy band, the pristine NiO_x shows a cliff of 10 meV while the NiO_x-EtOH introduces a spike of 80 meV that is favorable for effective carrier transport in PSC [36]. Fig. 5c displays the cross-sectional image of a complete PSC device. The image of PSC fabricated on ITO substrate (3.5×5 cm^2) is shown in inset in Fig. 5d. The *J-V* characteristics (Fig. 5d) and corresponding device parameters (Table 1) show the device results. The PSC with as-sputtered NiO_x achieved *PCE* of ~11.78% with J_{SC} ~18.94 $mAcm^{-2}$ and V_{OC} ~0.99 V. The device with EtOH/NiO_x demonstrated a higher device efficiency of ~13.52% (with higher J_{SC} ~19.48 $mAcm^{-2}$ and V_{OC} ~1.075 V) with device area of 1 cm^2. The statistics of device parameters (V_{OC} and *PCE*) are given in supporting information (Figs. 5e, f). The device parameters for NiO_x-EtOH are less scattered compared to the as-sputtered NiO_x indicating higher reproducibility. This is attributed to the improved quality of perovskite film (i.e., morphology, crystallinity) grown on NiO_x-EtOH (Fig. 4). The enhanced device parameters are attributed to the cumulative effect of deep HOMO level (Figs. 3a, b), improved hydrophilicity, and higher conductivity (induced by preferred crystal orientation (111) and XPS analysis) of NiO_x-EtOH. Moreover, we found that longer-time (>20 min) ethanol-treated NiO_x is detrimental to the device performance. This could be associated with poor interface quality induced by deteriorated NiO_x surface due to prolong interaction of ethanol and NiO_x surface. It is to be noted that although ethanol treatment of sputtered NiO_x film demonstrated an improvement in device performance, it is not as promising as solution-processed and high-

temperature annealed NiO_x [9,22,37]. Indeed, there is much room for improvement in device parameters to get competitive *PCE* for large area devices as in other reports [38,39].

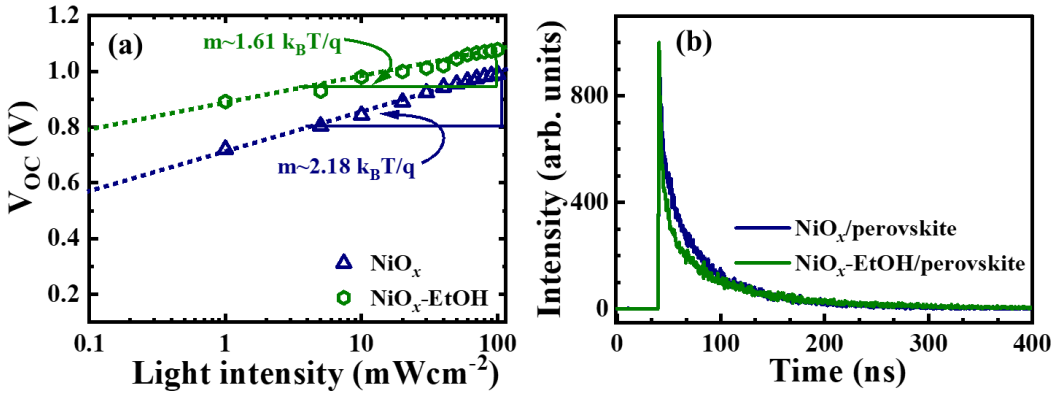

Fig. 6. The light intensity depended-V_{OC} of device (a). TRPL spectra of respective films (b).

To get insight into the recombination mechanism of photogenerated carriers in the device [40], we analysed the light intensity dependence of V_{OC}. Fig. 6a depicts a semi-logarithmic plot of V_{OC} as a function of light intensity. The linear fitting of the V_{OC}-I plot for the device with pristine NiO_x showed a slope of ~2.18 k_BT/q, which suggests a dominant Shockley–Read–Hall recombination via comparatively deep traps, which act as efficient recombination centers [26,40], While a lower value of slope (~1.61 k_BT/q) for the device with NiO_x-EtOH suggests comparatively attenuated trap-assisted recombination. The lower value of the diode ideality factor for the NiO_x-EtOH device supports an increase in V_{OC}. Although the diode quality of the perovskite device is better for the device with NiO_x-EtOH, both devices are limited by recombination via active trap states in perovskite bulk or at interfaces. There is much room for further improvement of the NiO_x/perovskite interface and bulk quality of PSCs. Furthermore, we evaluated the energy shift ($\Delta E = E_g - E_1$; E_1 is an intercept of the V_{OC}–I plot) [40]. It is calculated to be 0.636 eV for the device with NiO_x-EtOH which is lower than the as-sputtered NiO_x case (0.766 eV). It indicates a higher energetic disorder in the device near the interfacial layer of perovskite and as-sputtered NiO_x that is detrimental for interface quality.

To explore the HTL/perovskite interface, we measured TRPL spectroscopy. Fig. 6b shows the TRPL spectra of NiO_x/perovskite films. The carrier life time values are listed in Table 1. We observed a short carrier injection time (t_1 ~2.56 ns) for the NiO_x-EtOH/perovskite film (that for pristine NiO_x; ~4.68 ns). It suggests faster carrier transfer better carrier injection which is attributed to better interface quality [3,41]. This is correlated to modified surface morphology and chemistry of NiO_x-EtOH (as observed in SEM, XRD, and XPS results) confirmed by

growth characteristics. Similarly, a longer carrier life time (t_2 ~54.28 (43.31) ns for NiO_x-EtOH (pristine-NiO_x)/perovskite film) indicates an attenuated trap densities at interface and perovskite bulk. These TRPL results support an increase in V_{OC} and J_{SC} of the device with NiO_x-EtOH. This work underscores that the surface treatment of sputtered NiO_x film not only influences the properties of NiO_x films but also improves the film quality of perovskite grown on it. Indeed, there is still much room to improve the surface chemistry of sputtered NiO_x and interface and bulk quality of perovskite films grown for improvement of device performance.

4. Conclusions

In this work, we fabricated the perovskite device using sputtered NiO_x without annealing followed by surface treatment. The ethanol treatment on NiO_x modifies the film morphology, surface hydrophilicity, optophysical properties, and surface chemistry. We found that the NiO_x-EtOH film expedites the growth of good quality perovskite absorber which results in PCE of ~13.52% (device area of 1 cm^2) with higher reproducibility. The device analysis suggested that the device with NiO_x-EtOH film suppressed trap-assisted recombination in the perovskite bulk or interface as well as enhanced the carrier transport. This work substantiates that the surface treatment using multifunctional chemicals could be a nice choice for further optimization of properties of sputtered metal oxide film as an air-stable inorganic hole transport layer for the high efficiency and stable PSC.

Acknowledgments

D. B. Khadka acknowledges The Hitachi Global Foundation, Kurata Grant (#1391) for research funding. M. G. M. Pandian and A. R. M. A. thank National Institute for Materials Science, Japan and Anna University, Chennai/Flinders University, Australia for the International Cooperative Graduate Program fellowship. Authors thank to prof. G. Andersson (Flinders University) for his valuable suggestions.

Declaration of Competing Interest

The authors declare that they have no known competing financial interests or personal relationships that could have appeared to influence the work reported in this paper.

References

[1] J. Jeong, M. Kim, J. Seo, H. Lu, P. Ahlawat, A. Mishra, Y. Yang, M.A. Hope, F.T. Eickemeyer, M. Kim, Y.J. Yoon, I.W. Choi, B.P. Darwich, S.J. Choi, Y. Jo, J.H. Lee, B. Walker, S.M. Zakeeruddin, L. Emsley, U. Rothlisberger, A. Hagfeldt, D.S. Kim, M.

Grätzel, J.Y. Kim, Pseudo-halide anion engineering for α-FAPbI3 perovskite solar cells, Nature. 592 (2021) 381–385. https://doi.org/10.1038/s41586-021-03406-5.

[2] M. Saliba, M. Stolterfoht, C.M. Wolff, D. Neher, A. Abate, Measuring Aging Stability of Perovskite Solar Cells, Joule. 2 (2018) 1019–1024. https://doi.org/10.1016/j.joule.2018.05.005.

[3] D.B. Khadka, Y. Shirai, M. Yanagida, J.W. Ryan, K. Miyano, Exploring the effects of interfacial carrier transport layers on device performance and optoelectronic properties of planar perovskite solar cells, J. Mater. Chem. C. 5 (2017) 8819–8827. https://doi.org/10.1039/C7TC02822A.

[4] C. Bi, Q. Wang, Y. Shao, Y. Yuan, Z. Xiao, J. Huang, Non-wetting surface-driven high-aspect-ratio crystalline grain growth for efficient hybrid perovskite solar cells., Nat. Commun. 6 (2015) 7747. https://doi.org/10.1038/ncomms8747.

[5] J. You, L. Meng, T.-B. Song, T.-F. Guo, Y. (Michael) Yang, W.-H. Chang, Z. Hong, H. Chen, H. Zhou, Q. Chen, Y. Liu, N. De Marco, Y. Yang, Improved air stability of perovskite solar cells via solution-processed metal oxide transport layers, Nat. Nanotechnol. 11 (2016) 75–81. https://doi.org/10.1038/nnano.2015.230.

[6] D.B. Khadka, Y. Shirai, M. Yanagida, K. Miyano, Insights into Accelerated Degradation of Perovskite Solar Cells under Continuous Illumination Driven by Thermal Stress and Interfacial Junction, ACS Appl. Energy Mater. 4 (2021) 11121–11132. https://doi.org/10.1021/acsaem.1c02037.

[7] Z. Yang, B.H. Babu, S. Wu, T. Liu, S. Fang, Z. Xiong, L. Han, W. Chen, Review on Practical Interface Engineering of Perovskite Solar Cells: From Efficiency to Stability, Sol. RRL. 4 (2020) 1900257. https://doi.org/10.1002/solr.201900257.

[8] X. Yin, Y. Guo, H. Xie, W. Que, L.B. Kong, Nickel Oxide as Efficient Hole Transport Materials for Perovskite Solar Cells, Sol. RRL. 3 (2019) 1900001. https://doi.org/10.1002/solr.201900001.

[9] C.C. Boyd, R.C. Shallcross, T. Moot, R. Kerner, L. Bertoluzzi, A. Onno, S. Kavadiya, C. Chosy, E.J. Wolf, J. Werner, J.A. Raiford, C. de Paula, A.F. Palmstrom, Z.J. Yu, J.J. Berry, S.F. Bent, Z.C. Holman, J.M. Luther, E.L. Ratcliff, N.R. Armstrong, M.D. McGehee, Overcoming Redox Reactions at Perovskite-Nickel Oxide Interfaces to

Boost Voltages in Perovskite Solar Cells, Joule. 4 (2020) 1759–1775. https://doi.org/10.1016/j.joule.2020.06.004.

[10] S. Seo, S. Jeong, C. Bae, N.-G. Park, H. Shin, Perovskite Solar Cells with Inorganic Electron- and Hole-Transport Layers Exhibiting Long-Term (≈500 h) Stability at 85 °C under Continuous 1 Sun Illumination in Ambient Air, Adv. Mater. 30 (2018) 1801010. https://doi.org/10.1002/adma.201801010.

[11] R. Cheacharoen, C.C. Boyd, G.F. Burkhard, T. Leijtens, J.A. Raiford, K.A. Bush, S.F. Bent, M.D. McGehee, Encapsulating perovskite solar cells to withstand damp heat and thermal cycling, Sustain. Energy Fuels. 2 (2018) 2398–2406. https://doi.org/10.1039/C8SE00250A.

[12] W. Chen, F.Z. Liu, X.Y. Feng, A.B. Djurišić, W.K. Chan, Z.B. He, Cesium Doped NiOx as an Efficient Hole Extraction Layer for Inverted Planar Perovskite Solar Cells, Adv. Energy Mater. 7 (2017) 1700722. https://doi.org/10.1002/aenm.201700722.

[13] W.J. Scheideler, N. Rolston, O. Zhao, J. Zhang, R.H. Dauskardt, Rapid Aqueous Spray Fabrication of Robust NiO x : A Simple and Scalable Platform for Efficient Perovskite Solar Cells, Adv. Energy Mater. 9 (2019) 1803600. https://doi.org/10.1002/aenm.201803600.

[14] D. Di Girolamo, F. Matteocci, F.U. Kosasih, G. Chistiakova, W. Zuo, G. Divitini, L. Korte, C. Ducati, A. Di Carlo, D. Dini, A. Abate, Stability and Dark Hysteresis Correlate in NiO-Based Perovskite Solar Cells, Adv. Energy Mater. 9 (2019) 1901642. https://doi.org/10.1002/aenm.201901642.

[15] Y. Hou, E. Aydin, M. De Bastiani, C. Xiao, F.H. Isikgor, D.-J. Xue, B. Chen, H. Chen, B. Bahrami, A.H. Chowdhury, A. Johnston, S.-W. Baek, Z. Huang, M. Wei, Y. Dong, J. Troughton, R. Jalmood, A.J. Mirabelli, T.G. Allen, E. Van Kerschaver, M.I. Saidaminov, D. Baran, Q. Qiao, K. Zhu, S. De Wolf, E.H. Sargent, Efficient tandem solar cells with solution-processed perovskite on textured crystalline silicon, Science. 367 (2020) 1135–1140. https://doi.org/10.1126/science.aaz3691.

[16] M.B. Islam, M. Yanagida, Y. Shirai, Y. Nabetani, K. Miyano, NiO x Hole Transport Layer for Perovskite Solar Cells with Improved Stability and Reproducibility, ACS Omega. 2 (2017) 2291–2299. https://doi.org/10.1021/acsomega.7b00538.

[17] G. Li, Y. Jiang, S. Deng, A. Tam, P. Xu, M. Wong, H.-S. Kwok, Overcoming the Limitations of Sputtered Nickel Oxide for High-Efficiency and Large-Area Perovskite Solar Cells, Adv. Sci. 4 (2017) 1700463. https://doi.org/10.1002/advs.201700463.

[18] M. Yanagida, L. Shimomoto, Y. Shirai, K. Miyano, Effect of Carrier Transport in NiO on the Photovoltaic Properties of Lead Iodide Perovskite Solar Cells, Electrochemistry. 85 (2017) 231–235. https://doi.org/10.5796/electrochemistry.85.231.

[19] I. Hotový, D. Búc, Š. Haščík, O. Nennewitz, Characterization of NiO thin films deposited by reactive sputtering, Vacuum. 50 (1998) 41–44. https://doi.org/10.1016/S0042-207X(98)00011-6.

[20] E.L. Ratcliff, J. Meyer, K.X. Steirer, A. Garcia, J.J. Berry, D.S. Ginley, D.C. Olson, A. Kahn, N.R. Armstrong, Evidence for near-Surface NiOOH Species in Solution-Processed NiOx Selective Interlayer Materials: Impact on Energetics and the Performance of Polymer Bulk Heterojunction Photovoltaics, Chem. Mater. 23 (2011) 4988–5000. https://doi.org/10.1021/cm202296p.

[21] H.-L. Chen, Y.-S. Yang, Effect of crystallographic orientations on electrical properties of sputter-deposited nickel oxide thin films, Thin Solid Films. 516 (2008) 5590–5596. https://doi.org/10.1016/j.tsf.2007.07.035.

[22] S. Liu, R. Chen, X. Tian, Z. Yang, J. Zhou, F. Ren, S. Zhang, Y. Zhang, M. Guo, Y. Shen, Z. Liu, W. Chen, Boost the efficiency of nickel oxide-based formamidinium-cesium perovskite solar cells to 21% by using coumarin 343 dye as defect passivator, Nano Energy. 94 (2022) 106935. https://doi.org/10.1016/j.nanoen.2022.106935.

[23] J.W. Jung, C.-C. Chueh, A.K.-Y. Jen, A Low-Temperature, Solution-Processable, Cu-Doped Nickel Oxide Hole-Transporting Layer via the Combustion Method for High-Performance Thin-Film Perovskite Solar Cells, Adv. Mater. 27 (2015) 7874–7880. https://doi.org/10.1002/adma.201503298.

[24] N. Pant, M. Yanagida, Y. Shirai, K. Miyano, Effect of different surface treatments of sputtered NiO_x on the photovoltaic parameters of perovskite solar cells: a correlation study, Appl. Phys. Express. 13 (2020) 25505. https://doi.org/10.35848/1882-0786/ab6bde.

[25] M.B. Islam, N. Pant, M. Yanagida, Y. Shirai, K. Miyano, Effect of hydroxyl groups in

NiO x on the open circuit voltage of lead iodide perovskite solar cells, Jpn. J. Appl. Phys. 57 (2018) 08RE06. https://doi.org/10.7567/JJAP.57.08RE06.

[26] D.B. Khadka, Y. Shirai, M. Yanagida, T. Masuda, K. Miyano, Enhancement in efficiency and optoelectronic quality of perovskite thin films annealed in MACl vapor, Sustain. Energy Fuels. 1 (2017) 755–766. https://doi.org/10.1039/C7SE00033B.

[27] D.B. Khadka, Y. Shirai, M. Yanagida, K. Miyano, Unraveling the Impacts Induced by Organic and Inorganic Hole Transport Layers in Inverted Halide Perovskite Solar Cells, ACS Appl. Mater. Interfaces. 11 (2019) 7055–7065. https://doi.org/10.1021/acsami.8b20924.

[28] D. Dong, W. Wang, G. Dong, Y. Zhou, Z. Wu, M. Wang, F. Liu, X. Diao, Electrochromic properties of NiO :H films deposited by DC magnetron sputtering for ITO/NiO :H/ZrO2/WO3/ITO device, Appl. Surf. Sci. 357 (2015) 799–805. https://doi.org/10.1016/j.apsusc.2015.09.056.

[29] P. Salunkhe, M.A. A V, D. Kekuda, Investigation on tailoring physical properties of Nickel Oxide thin films grown by dc magnetron sputtering, Mater. Res. Express. 7 (2020) 016427. https://doi.org/10.1088/2053-1591/ab69c5.

[30] S. Siebentritt, Why are kesterite solar cells not 20% efficient?, Thin Solid Films. 535 (2013) 1–4. https://doi.org/10.1016/j.tsf.2012.12.089.

[31] M.C. Biesinger, L.W.M. Lau, A.R. Gerson, R.S.C. Smart, The role of the Auger parameter in XPS studies of nickel metal, halides and oxides, Phys. Chem. Chem. Phys. 14 (2012) 2434–2442. https://doi.org/10.1039/C2CP22419D.

[32] Y. Sun, W. Chen, Y. Wu, Z. He, S. Zhang, S. Chen, A low-temperature-annealed and UV-ozone-enhanced combustion derived nickel oxide hole injection layer for flexible quantum dot light-emitting diodes, Nanoscale. 11 (2019) 1021–1028. https://doi.org/10.1039/C8NR08976K.

[33] S. Liu, R. Liu, Y. Chen, S. Ho, J.H. Kim, F. So, Nickel Oxide Hole Injection/Transport Layers for Efficient Solution-Processed Organic Light-Emitting Diodes, Chem. Mater. 26 (2014) 4528–4534. https://doi.org/10.1021/cm501898y.

[34] G.Y. Kim, S.H. Oh, B.P. Nguyen, W. Jo, B.J. Kim, D.G. Lee, H.S. Jung, Efficient

carrier separation and intriguing switching of bound charges in inorganic-organic lead halide solar cells, J. Phys. Chem. Lett. 6 (2015) 2355–2362. https://doi.org/10.1021/acs.jpclett.5b00967.

[35] F. Liu, Q. Dong, M.K. Wong, A.B. Djurišić, A. Ng, Z. Ren, Q. Shen, C. Surya, W.K. Chan, J. Wang, A.M.C. Ng, C. Liao, H. Li, K. Shih, C. Wei, H. Su, J. Dai, Is Excess PbI 2 Beneficial for Perovskite Solar Cell Performance?, Adv. Energy Mater. 6 (2016) 1502206. https://doi.org/10.1002/aenm.201502206.

[36] G. Kapil, T.S. Ripolles, K. Hamada, Y. Ogomi, T. Bessho, T. Kinoshita, J. Chantana, K. Yoshino, Q. Shen, T. Toyoda, T. Minemoto, T.N. Murakami, H. Segawa, S. Hayase, Highly Efficient 17.6% Tin-Lead Mixed Perovskite Solar Cells Realized through Spike Structure, Nano Lett. 18 (2018) 3600–3607. https://doi.org/10.1021/acs.nanolett.8b00701.

[37] S. Wang, Y. Li, J. Yang, T. Wang, B. Yang, Q. Cao, X. Pu, L. Etgar, J. Han, J. Zhao, X. Li, A. Hagfeldt, Critical Role of Removing Impurities in Nickel Oxide on High-Efficiency and Long-Term Stability of Inverted Perovskite Solar Cells, Angew. Chemie Int. Ed. 61 (2022). https://doi.org/10.1002/anie.202116534.

[38] J. Peng, D. Walter, Y. Ren, M. Tebyetekerwa, Y. Wu, T. Duong, Q. Lin, J. Li, T. Lu, M.A. Mahmud, O.L.C. Lem, S. Zhao, W. Liu, Y. Liu, H. Shen, L. Li, F. Kremer, H.T. Nguyen, D.-Y. Choi, K.J. Weber, K.R. Catchpole, T.P. White, Nanoscale localized contacts for high fill factors in polymer-passivated perovskite solar cells, Science. 371 (2021) 390–395. https://doi.org/10.1126/science.abb8687.

[39] Z. Shen, Q. Han, X. Luo, Y. Shen, T. Wang, C. Zhang, Y. Wang, H. Chen, X. Yang, Y. Zhang, L. Han, Crystal-array-assisted growth of a perovskite absorption layer for efficient and stable solar cells, Energy Environ. Sci. 15 (2022) 1078–1085. https://doi.org/10.1039/D1EE02897A.

[40] S.R. Cowan, A. Roy, A.J. Heeger, Recombination in polymer-fullerene bulk heterojunction solar cells, Phys. Rev. B. 82 (2010) 245207. https://doi.org/10.1103/PhysRevB.82.245207.

[41] C.J. Hages, A. Redinger, S. Levcenko, H. Hempel, M.J. Koeper, R. Agrawal, D. Greiner, C.A. Kaufmann, T. Unold, Identifying the Real Minority Carrier Lifetime in

Nonideal Semiconductors: A Case Study of Kesterite Materials, Adv. Energy Mater. 7 (2017) 1700167. https://doi.org/10.1002/aenm.201700167.